


From Heisenberg to Hubbard: An initial state for the shallow quantum simulation of correlated electrons

Bruno Murta^{1,2,*} and J. Fernández-Rossier^{2,†}

¹*Departamento de Física, Universidade do Minho, Campus de Gualtar, 4710-057 Braga, Portugal*

²*International Iberian Nanotechnology Laboratory (INL), Avenida Mestre José Veiga, 4715-330 Braga, Portugal*

 (Received 1 November 2023; revised 22 December 2023; accepted 2 January 2024; published 16 January 2024)

The widespread use of the noninteracting ground state as the initial state for the digital quantum simulation of the Fermi-Hubbard model is largely due to the scarcity of alternative easy-to-prepare approximations to the exact ground state in the literature. Exploiting the fact that the spin- $\frac{1}{2}$ Heisenberg model is the effective low-energy theory of the Fermi-Hubbard model at half-filling in the strongly interacting limit, here we propose a three-step deterministic quantum routine to prepare an educated guess of the ground state of the Fermi-Hubbard model through a shallow circuit suitable for near-term quantum hardware. First, the ground state of the Heisenberg model is initialized via a hybrid variational method using an ansatz that explores only the correct symmetry subspace. Second, a general method is devised to convert a multi-spin- $\frac{1}{2}$ wave function into its fermionic version. Third, taking inspiration from the Baeriswyl ansatz, a constant-depth single-parameter layer that adds doublon-holon pairs is applied to this fermionic state. Numerical simulations on chains and ladders with up to 12 sites confirm the improvement over the noninteracting ground state of the overlap with the exact ground state for the intermediate values of the interaction strength at which quantum simulation is found to be most relevant. More broadly, the general scheme to convert a multi-spin- $\frac{1}{2}$ state into a half-filled fermionic state may bridge the gap between quantum spin models and lattice models of correlated fermions in the realm of digital quantum simulation.

DOI: [10.1103/PhysRevB.109.035128](https://doi.org/10.1103/PhysRevB.109.035128)

I. INTRODUCTION

Digital quantum simulation [1,2] is expected to become a leading method to study correlated electrons [3]. By exploiting the principle of superposition and the natural encoding of entanglement, quantum computers can represent the full wave function of quantum many-body systems in a scalable way, which may allow the properties that defy state-of-the-art numerical methods on conventional hardware to be probed [4,5]. A problem that offers the prospect of achieving such a quantum advantage [6,7], even with noisy intermediate-scale quantum (NISQ) processors [8], is the determination of the phase diagram of the Fermi-Hubbard model [9–11] by preparing the exact ground state of the second-quantized Hamiltonian

$$\hat{H} = -t \sum_{i,\tau} \sum_{\sigma=\uparrow,\downarrow} (\hat{c}_{i,\sigma}^\dagger \hat{c}_{i+\tau,\sigma} + \text{H.c.}) + U \sum_i \hat{n}_{i,\uparrow} \hat{n}_{i,\downarrow}, \quad (1)$$

where the sum over τ includes the nearest neighbors of site i , and $t > 0$ and $U > 0$ define the interaction strength $\frac{U}{t}$. The most challenging and relevant regime [12] of the Fermi-Hubbard model occurs when the two competing energy scales are comparable, i.e., the Hubbard parameter U is of the order of the bandwidth W of the underlying tight-binding model (e.g., $W = 4t$ in one dimension, $W = 8t$ for the square lattice).

A key requirement for any ground-state preparation method is an initial state with non-negligible overlap with the target state. In the case of the Fermi-Hubbard model, the standard choice is the noninteracting ground state [6,7], but its vanishing fidelity relative to the exact ground state [13] for the intermediate range $U \sim W$ calls for a more educated guess. Mean-field states [14] face the same issue, with the additional drawback of often breaking symmetries of the Hamiltonian. The Gutzwiller wave function [9] does produce a substantially greater overlap with the exact ground state at intermediate and large $\frac{U}{t}$, but the NISQ-friendly schemes proposed to initialize it [13,15] require, on average, a number of repetitions to succeed that becomes prohibitively large for a lattice of sufficiently great size due to their probabilistic nature.

Here we introduce a deterministic quantum routine that is suitable for NISQ hardware to prepare a better approximation than the noninteracting ground state of the exact ground state of the Fermi-Hubbard model at half-filling with intermediate or large $\frac{U}{t}$. This scheme makes use of the fact that, in the strongly interacting limit $\frac{U}{t} \rightarrow \infty$, the charge degrees of freedom are frozen and the Fermi-Hubbard model is reduced [3] to the antiferromagnetic spin- $\frac{1}{2}$ Heisenberg model [16],

$$\hat{H} = J \sum_{i,\tau} (\hat{S}_i^x \hat{S}_{i+\tau}^x + \hat{S}_i^y \hat{S}_{i+\tau}^y + \hat{S}_i^z \hat{S}_{i+\tau}^z), \quad (2)$$

with $J = \frac{4t^2}{U}$. This result is valid for any lattice at half-filling and may be extended to hopping terms beyond nearest neighbors. Although determining the ground state of the Heisenberg model is generally nontrivial, we can benefit from the smaller

*bpmurta@gmail.com

†On permanent leave from Departamento de Física Aplicada, Universidad de Alicante, 03690 San Vicente del Raspeig, Spain.

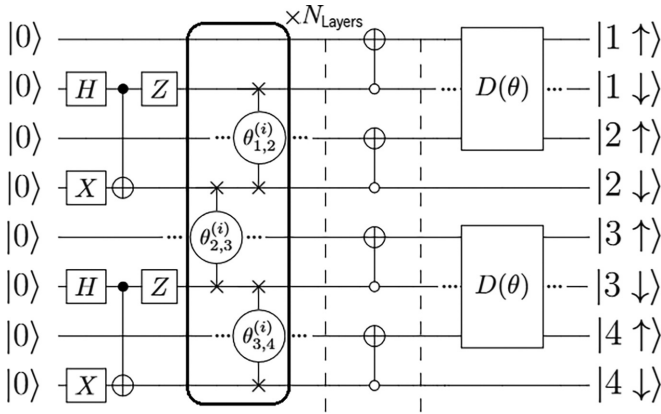


FIG. 1. Quantum circuit that prepares improved fermionic version of ground state of spin- $\frac{1}{2}$ Heisenberg model [16] on a lattice with $N = 4$ sites, which approximates the ground state of the Fermi-Hubbard model [9–11]. The first part (left of first dashed line) prepares the ground state of the Heisenberg model via VQE [21] using a N_{Layers} -layer ansatz that starts from a product state of valence bonds and explores the $S_{\text{Total}} = 0$ subspace [22]. The two-qubit building block of the ansatz is defined in Eq. (3). The second part converts this wave function into its $2N$ -qubit fermionic version, assuming the Jordan-Wigner transformation [23] is used. The third part (right of second dashed line) introduces pairs of empty and doubly occupied sites to this fermionic state. The two-qubit operation $D(\theta)$ is defined in Eq. (6). The ellipses before and after two-qubit operations indicate the middle qubit is idle.

size of the Hilbert space relative to the full-blown fermionic model to mitigate some of the most cumbersome issues faced in quantum simulation that arise from the exponential wall problem [17], namely, the orthogonality catastrophe [18] and the barren plateaus [19] in hybrid variational methods [20].

The quantum scheme herein put forth comprises three parts that can be identified in the circuit scheme shown in Fig. 1. The first part concerns the preparation of the ground state of the spin- $\frac{1}{2}$ Heisenberg model defined on an N -site balanced bipartite lattice via the variational quantum eigensolver (VQE) [21] with an ansatz that explores only the $S_{\text{Total}} = 0$ subspace [22]. The second part converts this N -spin- $\frac{1}{2}$ wave function into the respective fermionic state defined on $2N$ qubits, assuming the Jordan-Wigner transformation [23] is employed. The third part introduces pairs of empty and doubly-occupied sites in the fermionic version of the Heisenberg ground state. The remainder of this paper follows the construction of this three-step initial state preparation routine sequentially, with one section dedicated to each step. Numerical results of simulations on chains and ladders with up to 12 sites complement the explanations. The final section summarizes the main results and discusses potential further developments.

II. HYBRID VARIATIONAL PREPARATION OF GROUND STATE OF HEISENBERG MODEL

In the first part, the exact ground state of the antiferromagnetic spin- $\frac{1}{2}$ Heisenberg model on a given lattice with N sites is prepared via VQE. The building block of the ansatz is the eSWAP(θ) = $e^{-i\frac{\theta}{2}\text{SWAP}}$ [22], corresponding to the following

SU(2)-invariant two-qubit operation

$$\begin{pmatrix} e^{-i\frac{\theta}{2}} & 0 & 0 & 0 \\ 0 & \cos\frac{\theta}{2} & -i\sin\frac{\theta}{2} & 0 \\ 0 & -i\sin\frac{\theta}{2} & \cos\frac{\theta}{2} & 0 \\ 0 & 0 & 0 & e^{-i\frac{\theta}{2}} \end{pmatrix} \equiv \begin{array}{c} \text{---} \times \text{---} \\ \text{---} \theta \text{---} \\ \text{---} \times \text{---} \end{array}. \quad (3)$$

The basis gate decomposition of the eSWAP can be found in Appendix A. Starting from a reference state with the expected S_{Total} and S_{Total}^z for the exact ground state ensures the manifold spanned by the parameterized state is confined to the subspace defined by these good quantum numbers. In particular, for a balanced bipartite lattice, the Lieb-Mattis theorem [24] guarantees that the ground state of the antiferromagnetic spin- $\frac{1}{2}$ Heisenberg model has $S_{\text{Total}} = S_{\text{Total}}^z = 0$, so an appropriate reference state motivated by the ease of preparation is a product state of valence bonds $\frac{|\uparrow\downarrow\rangle - |\downarrow\uparrow\rangle}{\sqrt{2}}$ at the odd-even pairs (1, 2), (3, 4), ..., (N-1, N) of adjacent qubits in a linear configuration. On top of this reference state, N_{Layers} layers of the ansatz are applied, each corresponding to the execution of $\frac{N}{2} - 1$ eSWAPs at the even-odd pairs of qubits, followed by the implementation of $\frac{N}{2}$ eSWAPs at the odd-even pairs (see Fig. 1). The structure of the ansatz is defined such that even in the most restrictive case of linear qubit connectivity no rerouting of qubits is required to implement it. Although previous works [25–27] have motivated this ansatz in the spirit of discretized adiabatic evolution [28,29], here we follow its interpretation [22] as a generator of resonating-valence-bond (RVB) states [30,31], in which case each eSWAP is assigned its own free parameter, resulting in a total of $N_{\text{Layers}}(N-1)$ parameters. Henceforth, this ansatz will be referred to as *RVB-inspired ansatz*. Since the first step is the only potential bottleneck of this scheme, *in silico* noiseless simulations were performed to assess the scalability of the preparation of the ground state of the spin- $\frac{1}{2}$ Heisenberg model via VQE. The details of the optimization of the parameters of the ansatz can be found in Appendix B. Two lattice geometries were considered: $L \times 1$ (i.e., chains) and $L \times 2$ (i.e., ladders). The total number of lattice sites— $N = L$ and $N = 2L$, respectively—was at most 12. Open boundary conditions were considered in all cases, but periodic boundary conditions could be adopted as well, though the scaling of the number of layers with the system size may not be as favorable (see Supplemental Material, SM [32], and Ref. [25]). The total number of sites was chosen to be even to ensure that the ground state is a singlet. The true ground state was determined via exact diagonalization [33], which allowed us to calculate the infidelity, $1 - |\langle\psi_0|\psi_{\text{RVB}}\rangle|^2$, between the exact ground state, $|\psi_0\rangle$, and the optimized RVB-inspired ansatz, $|\psi_{\text{RVB}}\rangle$, for a given N_{Layers} . Despite having access to $|\psi_0\rangle$, the cost function adopted in the optimization of $|\psi_{\text{RVB}}\rangle$ was the energy instead of $|\langle\psi_0|\psi_{\text{RVB}}\rangle|^2$, as the former is a more scalable option.

The results are shown in Fig. 2. As expected, for a fixed N_{Layers} , the infidelity relative to the exact ground state increases as the lattice size grows. Conversely, increasing N_{Layers} for a given lattice produces a closer approximation to the true ground state. Importantly, as shown in the tables below the respective graphs, the minimum number of layers required to achieve an infidelity of at most 0.01 increases linearly with

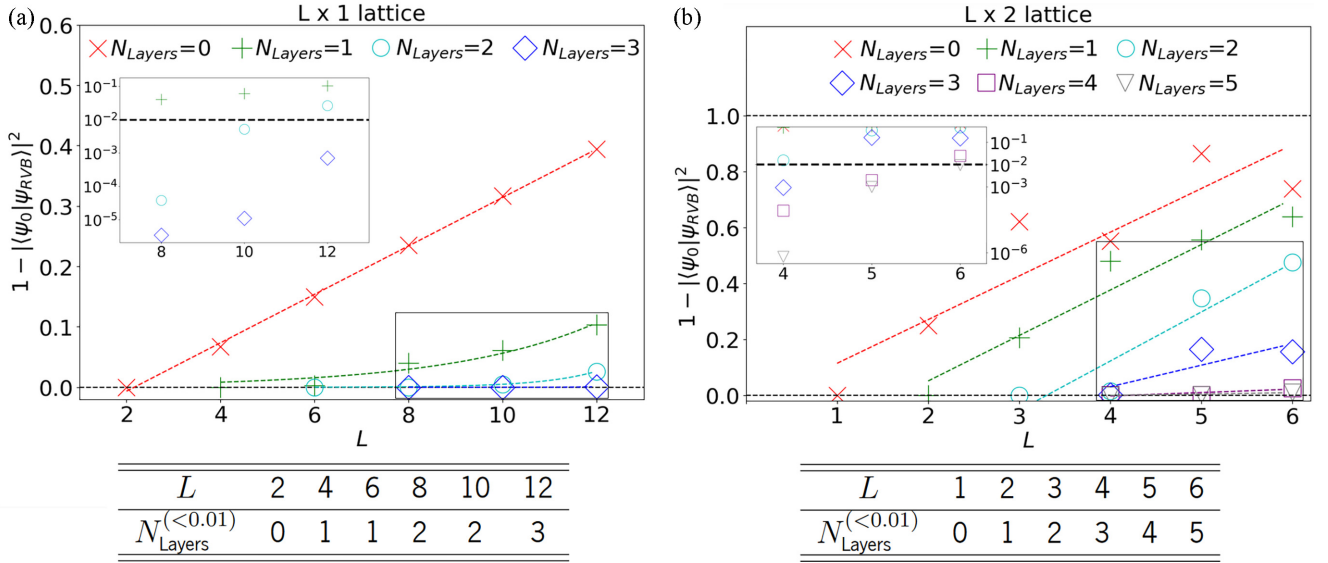


FIG. 2. Infidelity between exact ground state and RVB-inspired ansatz [22] obtained via VQE [21] for antiferromagnetic spin- $\frac{1}{2}$ Heisenberg model [16] in chains (a) and ladders (b) with up to 12 sites and open boundary conditions. The inset plots are a zoomed-in view (with the vertical axis in logarithmic scale) of the highlighted rectangular section in the bottom-right corner of the main plot. The axes labels of the insets were not included due to lack of space, but they coincide with those of the main plots. The tables below each graph present the minimum number of layers of the RVB-inspired ansatz to achieve an infidelity below 0.01 with respect to the exact ground state. The dashed lines in the main plots are just a guide to the eye. As expected, as the number of lattice sites increases, more ansatz layers are required to achieve a given infidelity target. $N_{\text{Layers}} = 0$ corresponds to the product state of valence bonds that is the input state of the RVB-inspired ansatz (see Fig. 1).

the number of lattice sites, and the prefactor is small. For example, the three-layer RVB-inspired ansatz that approximates the exact ground state of the Heisenberg model on a 12-site chain with fidelity 0.9993 takes only 19 CNOTs of depth, which is less than the 22 CNOTs of depth required to prepare the noninteracting ground state of the corresponding Fermi-Hubbard model [34,35]. As for the 6×2 ladder, the 5 layers of the RVB-inspired ansatz that produce a fidelity of 0.991 take 31 CNOTs of depth, which is not significantly above the 22 CNOTs needed to prepare the noninteracting ground state of the Fermi-Hubbard model [34,35]. Hence, assuming the observed trend continues for larger lattices, the resulting circuits should be shallow enough for NISQ hardware.

III. CONVERSION OF MULTI-SPIN- $\frac{1}{2}$ STATE INTO HALF-FILLED FERMIONIC STATE

We now proceed to the second part of the quantum scheme, where the N -spin- $\frac{1}{2}$ ground state of the Heisenberg model is converted into a $2N$ -qubit fermionic state that is the exact ground state of the Fermi-Hubbard model on the same lattice at half-filling in the $\frac{U}{t} \rightarrow \infty$ limit. This conversion is valid for any multi-spin- $\frac{1}{2}$ state.

Let us first consider a generic single-spin- $\frac{1}{2}$ state $|\psi^{\text{spin}}\rangle = a|\uparrow\rangle + b|\downarrow\rangle \equiv a|0\rangle + b|1\rangle$. The corresponding single-site fermionic state is $|\psi^{\text{fermion}}\rangle = a|10\rangle + b|01\rangle$, where the Jordan-Wigner transformation [23] is implicit. If we add an ancillary qubit in $|0\rangle$ to $|\psi^{\text{spin}}\rangle$, as in $|0\rangle \otimes |\psi^{\text{spin}}\rangle = a|00\rangle + b|01\rangle$, the two-qubit operation that must be applied to transform $|0\rangle \otimes |\psi^{\text{spin}}\rangle$ into $|\psi^{\text{fermion}}\rangle$ should map $|00\rangle$ to $|10\rangle$

while leaving $|01\rangle$ unchanged. Its action on the remaining two basis states is immaterial [36]. Hence, a valid choice is

$$\begin{pmatrix} 0 & 0 & 1 & 0 \\ 0 & 1 & 0 & 0 \\ 1 & 0 & 0 & 0 \\ 0 & 0 & 0 & 1 \end{pmatrix} \equiv \begin{array}{c} \text{---} \oplus \text{---} \\ | \\ \text{---} \circ \text{---} \end{array}, \quad (4)$$

where the top qubit in the diagram is the most significant [37], and the unfilled circle means the NOT gate is triggered only when the control qubit is $|0\rangle$.

The generalization to an arbitrary number of lattice sites is straightforward, apart from the extra minus signs, due to the anticommutation relations of fermionic operators. Actually, these fermionic signs only arise when the qubits are ordered by spin instead of site. Indeed, in the latter case, the amplitudes of $|\psi^{\text{fermion}}\rangle$ are exactly equal to those of $|\psi^{\text{spin}}\rangle$. For example, a basis state of the form $|\uparrow\downarrow\downarrow\uparrow\downarrow\uparrow\rangle$ corresponds explicitly to $|\uparrow\rangle_1 \otimes |\downarrow\rangle_2 \otimes |\downarrow\rangle_3 \otimes |\uparrow\rangle_4 \otimes |\downarrow\rangle_5 \otimes |\uparrow\rangle_6$, the fermionic version of which is naturally ordered by site as well: $\hat{c}_{1,\uparrow}^\dagger \hat{c}_{2,\downarrow}^\dagger \hat{c}_{3,\downarrow}^\dagger \hat{c}_{4,\uparrow}^\dagger \hat{c}_{5,\downarrow}^\dagger \hat{c}_{6,\uparrow}^\dagger |\Omega\rangle$, where $|\Omega\rangle$ denotes the vacuum state. Hence, ordering the $2N$ qubits by site, the conversion of $|\psi^{\text{spin}}\rangle$ into $|\psi^{\text{fermion}}\rangle$ amounts to repeating the application of the two-qubit operation stated in Eq. (4) at all pairs of qubits encoding a lattice site (see Fig. 1).

If the qubits are ordered by spin instead, returning to the example above, upon commuting the creation operators we obtain $-\hat{c}_{1,\uparrow}^\dagger \hat{c}_{4,\uparrow}^\dagger \hat{c}_{6,\uparrow}^\dagger \hat{c}_{2,\downarrow}^\dagger \hat{c}_{3,\downarrow}^\dagger \hat{c}_{5,\downarrow}^\dagger |\Omega\rangle$, so an extra minus sign must be applied to its amplitude. If S_{Total}^z is a good quantum number, fermionic signs can be accounted for by replacing

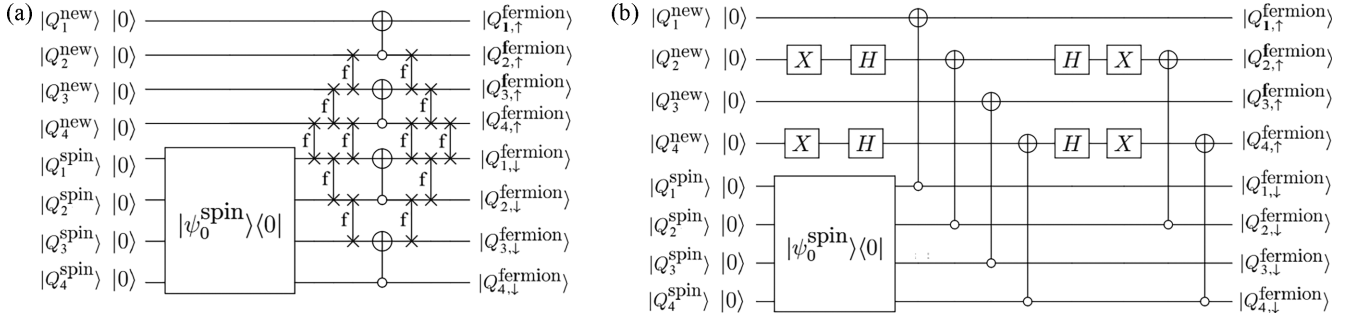


FIG. 3. Quantum circuit to transform N -spin- $\frac{1}{2}$ wave function $|\psi_0^{\text{spin}}\rangle$ into spin- $\frac{1}{2}$ fermionic wave function on lattice of $N = 4$ sites at half-filling with qubits ordered by spin for linear qubit connectivity (a) and all-to-all qubit connectivity (b). The latter case results in a constant circuit depth overhead of just two CNOTs but only works if S_{Total}^z is a good quantum number of $|\psi_0^{\text{spin}}\rangle$. If this is not the case, then the $O(N)$ -depth circuit in (a) must be considered even if there are no connectivity constraints.

Eq. (4) at every other site with

$$\begin{pmatrix} 0 & 0 & 1 & 0 \\ 0 & 1 & 0 & 0 \\ -1 & 0 & 0 & 0 \\ 0 & 0 & 0 & 1 \end{pmatrix} \equiv \begin{array}{c} \text{---} X \text{---} H \text{---} \oplus \text{---} H \text{---} X \text{---} \oplus \text{---} \\ | \\ \text{---} \oplus \text{---} \\ | \\ \text{---} \oplus \text{---} \end{array}, \quad (5)$$

resulting in a constant-depth overhead as well. In case the input state involves basis states with different S_{Total}^z , a network of fermionic SWAPS [38] is required to prepare the spin-ordered fermionic state, as illustrated in Fig. 3 for $N = 4$ lattice sites.

IV. ADDITION OF DOUBLON-HOLON PAIRS

The third and final part of the quantum routine aims to increase the overlap of the fermionic Heisenberg ground state $|\psi_0^{(U/t \rightarrow \infty)}\rangle$ with the exact ground state of the Fermi-Hubbard model at finite $\frac{U}{t}$. A layer of two-qubit operations $D(\theta)$ with a single free parameter θ is applied to $|\psi_0^{(U/t \rightarrow \infty)}\rangle$. In the spirit of the Baeriswyl wave function [39], this layer promotes the hopping of spin- \uparrow electrons between adjacent odd-even pairs of sites (see Fig. 1) to give rise to doublon-holon pairs:

$$\begin{aligned} D(\theta)|\uparrow, \uparrow\rangle &= |\uparrow, \uparrow\rangle, & D(\theta)|\downarrow, \downarrow\rangle &= |\downarrow, \downarrow\rangle, \\ D(\theta)|\uparrow, \downarrow\rangle &= \cos \frac{\theta}{2} |\uparrow, \downarrow\rangle + \sin \frac{\theta}{2} |0, \uparrow\downarrow\rangle, \\ D(\theta)|\downarrow, \uparrow\rangle &= \cos \frac{\theta}{2} |\downarrow, \uparrow\rangle - \sin \frac{\theta}{2} |\uparrow\downarrow, 0\rangle. \end{aligned} \quad (6)$$

The basis gate decomposition of $D(\theta)$ can be found in Appendix A. The physical motivation behind this heuristic layer is that a lower interaction strength $\frac{U}{t}$ makes basis states with doubly occupied and empty sites less energetically costly, so the optimal θ found by minimizing the energy of the ansatz should increase monotonically with $\frac{U}{t}$, thus better approximating the exact ground state.

Crucially, the expected improvement of the fidelity with the exact ground state is only observed if $D(\theta)$ is applied to the qubits encoding the $|i, \uparrow\rangle$ and $|i+1, \uparrow\rangle$ orbitals with $|i, \downarrow\rangle$ between them (see Fig. 1). Expanding $D(\theta)$ in the Pauli basis and applying the Jordan-Wigner transformation [23] in

reverse, we obtain in this case

$$\begin{aligned} D(\theta) &= \frac{1 + \cos \frac{\theta}{2}}{2} + \frac{1 - \cos \frac{\theta}{2}}{2} (1 - 2\hat{n}_{i,\uparrow})(1 - 2\hat{n}_{i+1,\uparrow}) \\ &\quad - \sin \frac{\theta}{2} [\hat{c}_{i,\uparrow}(1 - 2\hat{n}_{i,\downarrow})\hat{c}_{i+1,\uparrow}^\dagger + \hat{c}_{i,\uparrow}^\dagger(1 - 2\hat{n}_{i,\downarrow})\hat{c}_{i+1,\uparrow}]. \end{aligned} \quad (7)$$

If $|i, \uparrow\rangle$ and $|i+1, \uparrow\rangle$ are adjacent instead, the $Z_{i,\downarrow} \equiv 1 - 2\hat{n}_{i,\downarrow}$ operators are absent from the spin- \uparrow hopping terms, which gives rise to a phase shift of -1 between the original basis states with only singly-occupied sites and the newly added ones with empty and doubly-occupied sites. This minus sign inhibits any improvement of the overlap with the exact ground state. For the sake of clarity, this point is illustrated with the Fermi-Hubbard dimer in Appendix C.

Figure 4 shows the improvement of the fidelity relative to the Fermi-Hubbard model ground state of the fermionic version of the Heisenberg ground state—prepared via the RVB-inspired ansatz with the minimum number of layers to achieve a fidelity of at least 0.99 (see Fig. 2)—upon applying this layer with a single parameter θ for the 12-site chain and ladder. Similar results were obtained for smaller chains and ladders (see SM [32]). Remarkably, the convex θ vs $\frac{U}{t}$ curves (shown in insets) obtained for chains and ladders of different sizes match almost perfectly (see Appendix D), so this parameter does not have to be optimized through a hybrid scheme. In fact, the results presented in Fig. 4 were obtained using the optimized θ from the simulations with the 10-site lattices of the same geometry. Importantly, the improved fermionic Heisenberg state outperforms the noninteracting ground state for $\frac{U}{t} \gtrsim 4$ —well within the most relevant regime of the Fermi-Hubbard model—and even goes beyond the Gutzwiller wave function for a larger $\frac{U}{t}$.

V. DISCUSSION AND CONCLUSION

Before we conclude, a critical analysis of the scalability of this three-step initial state preparation scheme is justified. The third step addresses the absence of charge fluctuations in the ground state of the spin- $\frac{1}{2}$ model with a negligible depth overhead and no repetition overhead at all. However, other variants may be explored in the future to produce a greater improvement of the fidelity relative to the exact ground state

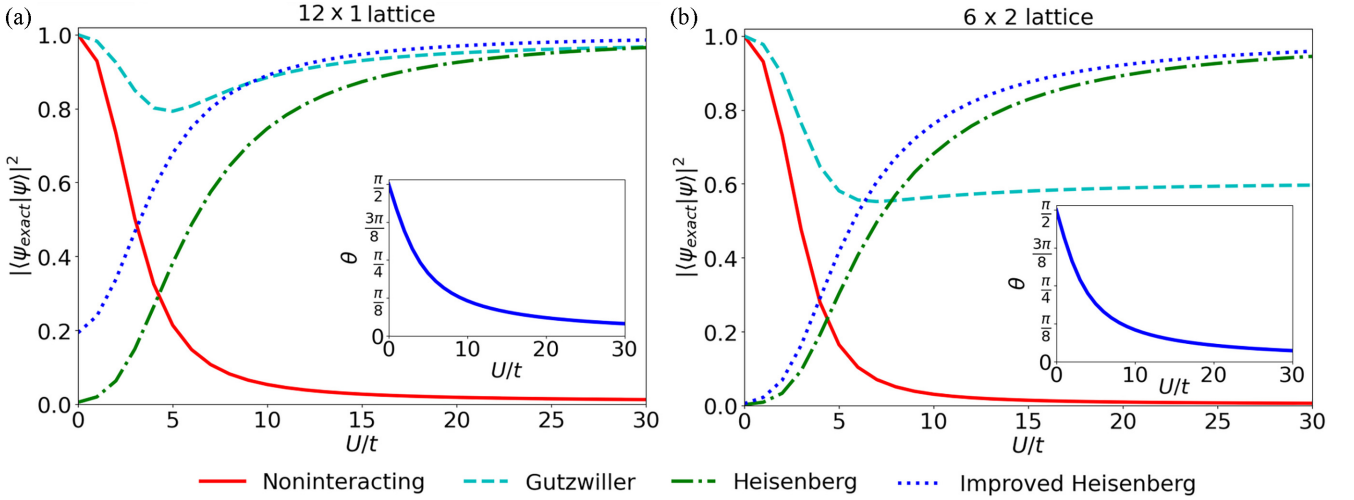


FIG. 4. Fidelity relative to the exact ground state of the Fermi-Hubbard model of the noninteracting ground state (red solid line), Gutzwiller wave function [9] (cyan dashed line), fermionic version of the Heisenberg ground state (green dashed-dotted line), and its improved version via the addition of doublon-holon pairs with a layer with a single free parameter θ (blue dotted line) for 12×1 (a) and 6×2 (b) lattices. The RVB-inspired ansatz with the minimum number of layers to achieve a fidelity of at least 0.99 was used to initialize the Heisenberg ground state (see Fig. 2). Open boundary conditions were considered. The insets show the optimized free parameter θ against the interaction strength $\frac{U}{t}$. Identical θ vs $\frac{U}{t}$ were obtained for smaller lattices. In fact, the values of θ used for these 12-site-lattice simulations were obtained from the simulations with 10-site lattices of the same geometry.

of the Fermi-Hubbard model in two dimensions. Regarding the first step, although the scaling of the number of layers of the RVB-inspired ansatz with the size of the ladders shown in Fig. 2(b) seems to be slow enough for NISQ hardware, numerical simulations on larger two-dimensional lattices are required to confirm this trend. Even if the exact ground state of a local Hamiltonian can only be approximated in terms of a long-range RVB state, in principle $\mathcal{O}(\text{poly}(N))$ layers suffice to generate such long-ranged valence bonds (see Appendix C of Ref. [22]). Importantly, the general character of the second step of this scheme allows one to take advantage of any accurate approximation of the ground state of a quantum spin- $\frac{1}{2}$ model (regardless of the ansatz employed) to approximate the ground state of the corresponding Fermi-Hubbard model for a sufficiently large interaction strength, thus bridging the gap between quantum spin models and lattice models of correlated electrons in digital quantum simulation.

In summary, we have developed a scheme to prepare an educated guess of the ground state of the Fermi-Hubbard model that may be adopted as the initial state on NISQ hardware. Further developments that we anticipate include simulations on nonbipartite lattices, possibly modifying the reference state of the RVB-inspired ansatz to probe the right symmetry subspace (e.g., replacing a valence bond with a triplet to set $S_{\text{Total}} = 1$); the consideration of the spin- $\frac{1}{2}$ model that includes $\mathcal{O}(t^4/U^3)$ ring-exchange terms in the VQE simulation; the exploration of analytical results to bypass the VQE simulation altogether, e.g., Bethe ansatz states [40–42] in one-dimensional (1D), Majumdar-Ghosh [43,44], and Shastry-Sutherland [45,46] states upon adding next-nearest-neighbor hopping terms in one and two dimensions, respectively; and the extension of the scheme beyond half-filling, e.g., replacing the Heisenberg model with the t-J model [3] or changing the particle number through a chemical potential term.

ACKNOWLEDGMENTS

B.M. acknowledges financial support from Fundação para a Ciência e a Tecnologia (FCT)–Portugal through Ph.D. Scholarship No. SFRH/BD/08444/2020. J.F.R. acknowledges financial support from FCT (Grant No. PTDC/FIS-MAC/2045/2021), the Generalitat Valenciana funding No. Prometeo2021/017 and No. MFA/2022/045, and funding from MICIIN-Spain (Grants No. PID2019-109539GB-C41 and No. PID2022-141712NB-C22).

APPENDIX A: BASIS GATE DECOMPOSITIONS

The basis gate decomposition of the eSWAP(θ) [see Eq. (3)], the building block of the RVB-inspired ansatz considered in the first step (see Fig. 1) of the three-step initial state preparation method herein introduced, is

$$\begin{array}{c} \left[U\left(\frac{\pi}{2}, \frac{\pi}{2}, 0\right) \right] \text{---} \left[U\left(\frac{\theta}{2}, \frac{\pi}{2}, \frac{\pi}{2}\right) \right] \text{---} \left[U\left(\frac{\theta}{2}, -\frac{\pi}{2}, \frac{\pi}{2}\right) \right] \text{---} \left[U\left(\frac{\pi}{2}, -\pi, 0\right) \right] \\ \left[U\left(0, 0, \frac{\pi}{2}\right) \right] \oplus \left[U\left(\frac{\theta}{2}, -\frac{\pi}{2}, -\pi\right) \right] \oplus \left[\frac{\pi}{2}, -\pi, -\frac{\pi}{2} \right] \oplus \left[U\left(\frac{\pi}{2}, \frac{\pi}{2}, 0\right) \right] \end{array}, \quad (\text{A1})$$

where the general single-qubit operation $U(\alpha, \beta, \gamma)$ is [47]

$$U(\alpha, \beta, \gamma) = \begin{pmatrix} \cos(\alpha/2) & -e^{i\gamma} \sin(\alpha/2) \\ e^{i\beta} \sin(\alpha/2) & e^{i(\beta+\gamma)} \cos(\alpha/2) \end{pmatrix}. \quad (\text{A2})$$

Similarly, the two-qubit operation $D(\theta)$ [see Eq. (6)], which adds doublon-holon pairs to the fermionic version of the Heisenberg ground state in the third step, can be decomposed in terms of elementary gates as follows:

$$\begin{array}{c} \left[U\left(\frac{\pi}{2}, -\pi, \frac{5\pi}{8}\right) \right] \text{---} \left[U\left(\frac{\theta}{2}, 0, 0\right) \right] \text{---} \left[U\left(\frac{\pi}{2}, -\frac{5\pi}{8}, -\pi\right) \right] \\ \left[U\left(0, 0, \frac{5\pi}{8}\right) \right] \oplus \left[U\left(\pi - \frac{\theta}{2}, 0, 0\right) \right] \oplus \left[\pi, 0, -\frac{3\pi}{8} \right] \end{array}. \quad (\text{A3})$$

APPENDIX B: OPTIMIZATION OF RVB-INSPIRED ANSATZ

The ground state of the antiferromagnetic spin- $\frac{1}{2}$ Heisenberg model was determined via VQE [21] using the RVB-inspired ansatz defined in Fig. 1. The parameters were optimized by minimizing the energy. Even though in the numerical simulations considered in this work we have access to the exact ground state obtained by diagonalizing the many-body Hamiltonian, the cost function considered in this optimization process was the energy and not the fidelity relative to the exact ground state, since for larger systems the exact ground state would not be known in advance.

The `scipy.optimize.minimize` function [48] was used to optimize the free parameters of the RVB-inspired ansatz. Since all parameters were bounded to the $[0, 2\pi]$ interval, this function implemented the sequential least squares programming (SLSQP) method. For a sufficiently large number of sites N , the optimization landscape became complex enough for the optimizer to become trapped in local minima for multiple sets of initial conditions. A twofold strategy was adopted to overcome this issue. First, after having optimized the $(N_{\text{Layers}} - 1)$ -layer ansatz, which resulted in a set of $(N_{\text{Layers}} - 1)(N - 1)$ parameter values $\vec{\theta}_{N_{\text{Layers}}-1}$, the initial conditions for the next step corresponding to the optimization of the N_{Layers} -layer ansatz were set as $\vec{\theta}_{N_{\text{Layers}}}^{\text{init}} = (\vec{\theta}_{N_{\text{Layers}}-1}, \vec{0})$, where $\vec{0}$ is a $(N - 1)$ -dimensional vector with all entries set to zero. The key point is that a layer of the RVB-inspired ansatz with all parameters set to zero amounts to the identity, so this corresponds to a layer-by-layer strategy where the outcome of one iteration is used as the starting point of the next. Second, to avoid being trapped in this initial state (which is often associated with a local minimum of the optimization landscape), a random value in the range $[-2\eta\pi, 2\eta\pi]$ —with $\eta \in [0, 1/2]$ a simulation parameter—was added to every entry of $\vec{\theta}_{N_{\text{Layers}}}^{\text{init}}$. In practice, five different values of the noise parameter, $\eta \in \{0.1, 0.2, 0.3, 0.4, 0.5\}$, were considered, with $N_{\text{reps}} = 10$ repetitions performed for each. Hence, for each

lattice geometry and every N_{Layers} , a total of 50 trials of the optimization process were carried out, each involving the optimization of all $N_{\text{Layers}}(N - 1)$ parameters. In the end, the trial that produced the lowest energy was selected per the variational principle, and the corresponding optimized parameters were stored. The final ansatz corresponds to the RVB-inspired ansatz with the optimized parameters associated with the best (i.e., lowest-energy) trial.

We note that no statistical analysis was involved in this optimization process and no outliers in the trials had to be excluded manually. The estimation of the energy of the parameterized state was performed via explicit matrix-vector multiplications using the full representation of the wave function, instead of sampling the Pauli strings with nonzero weight in the Hamiltonian. No noise model was adopted in these *in silico* simulations.

APPENDIX C: ADDING DOUBLON-HOLON PAIRS: FERMI-HUBBARD DIMER

As noted in Sec. IV, upon applying the two-qubit $D(\theta)$ operations to introduce charge fluctuations in the fermionic version of the ground state of the Heisenberg model, $|\psi_0^{(U/t \rightarrow \infty)}\rangle$, it turns out that having the $|i, \downarrow\rangle$ qubit between the $(|i, \uparrow\rangle, |i + 1, \uparrow\rangle)$ qubits on which $D(\theta)$ acts nontrivially is decisive to obtain the expected improvement of the overlap with the exact ground state at finite $\frac{U}{t}$ with respect to $|\psi_0^{(U/t \rightarrow \infty)}\rangle$. This is made clear by considering the Fermi-Hubbard dimer (i.e., a 2×1 lattice). In this case, $|\psi_0^{(U/t \rightarrow \infty)}\rangle = \frac{1}{\sqrt{2}}(|\uparrow, \downarrow\rangle - |\downarrow, \uparrow\rangle)$ (i.e., $N_{\text{Layers}} = 0$ in the RVB-inspired ansatz presented in Fig. 1). The exact ground state at an arbitrary interaction strength $\frac{U}{t}$ is given by

$$|\psi_{\text{exact}}\rangle = \mathcal{N} \left[\alpha \frac{|\uparrow, \downarrow\rangle - |\downarrow, \uparrow\rangle}{\sqrt{2}} + \frac{|\uparrow\downarrow, 0\rangle + |0, \uparrow\downarrow\rangle}{\sqrt{2}} \right], \quad (\text{C1})$$

where $\alpha = \frac{U + \sqrt{U^2 + 16t^2}}{4t}$, $\mathcal{N} = \frac{1}{\sqrt{1 + \alpha^2}}$ normalizes the wave function, and the basis states are ordered by site instead of

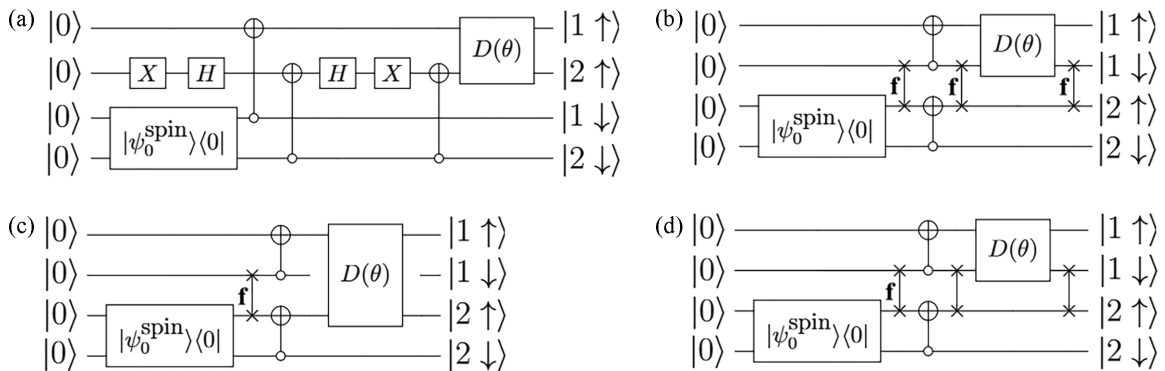


FIG. 5. Unsuccessful (a), (b) and successful (c), (d) implementations of the heuristic parameterized layer to improve the overlap of the fermionic version of the Heisenberg ground state with the exact ground state of the Fermi-Hubbard dimer at finite $\frac{U}{t}$. $D(\theta)$ is defined in Eq. (A3). Circuits in (a) and (c) assume all-to-all connectivity, while those in (b) and (d) are restricted to linear connectivity. The improvement of the overlap with the exact ground state at finite $\frac{U}{t}$ for an optimized parameter θ only occurs when the qubit that encodes the occupation of the spin- \downarrow orbital at site 1 is between the two qubits encoding the spin- \uparrow orbitals on which $D(\theta)$ acts nontrivially. Notice the subtle difference between (b) and (d): in the former (unsuccessful) case, the moving qubit is rerouted with fermionic SWAPS, while in the later (successful) case, the qubit rerouting is performed with conventional SWAPS.

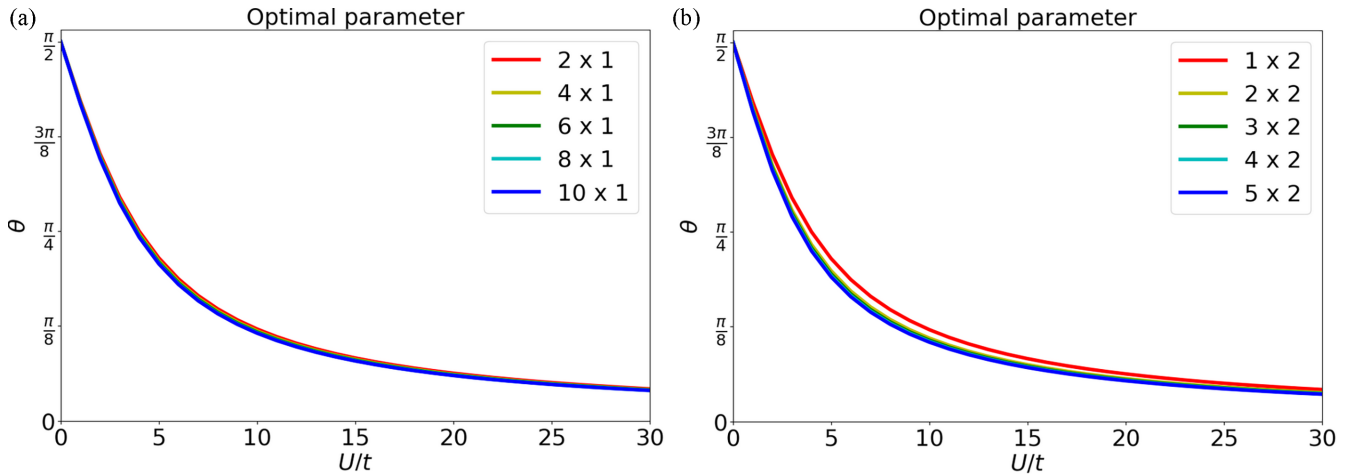


FIG. 6. Optimal value of free parameter θ of constant-depth layer that adds doublon-holon pairs to fermionic version of Heisenberg ground state for $L \times 1$ (a) and $L \times 2$ (b) lattices. θ decreases monotonically with $\frac{U}{t}$, resulting in a simple convex landscape. The θ vs $\frac{U}{t}$ profiles for lattices with the same geometry but different sizes are nearly coincident.

spin. However, upon applying $D(\theta)$ at the pair of adjacent qubits ($|1 \uparrow\rangle, |2 \uparrow\rangle$) of $|\psi_0^{(U/t \rightarrow \infty)}\rangle$ [see Figs. 5(a) and 5(b)], we obtain the following state:

$$\cos \frac{\theta}{2} \left(\frac{|\uparrow, \downarrow\rangle - |\downarrow, \uparrow\rangle}{\sqrt{2}} \right) - \sin \frac{\theta}{2} \left(\frac{|\uparrow\downarrow, 0\rangle + |0, \uparrow\downarrow\rangle}{\sqrt{2}} \right). \quad (\text{C2})$$

Were it not for the relative phase factor of $-1 = e^{i\pi}$ between the left-hand-side part involving only half-filled sites and the right-hand-side part with doublon-holon pairs, this ansatz would give rise to an exact representation of the true ground state of the Fermi-Hubbard dimer at any $\frac{U}{t}$ for a suitable choice of θ [cf. Eq. (C1)]. To remove this minus sign, we can instead apply the same two-qubit operation $D(\theta)$ but with the qubit encoding the spin- \downarrow orbital at site 1 between the two qubits on which $D(\theta)$ acts nontrivially, as shown in Figs. 5(c) and 5(d). The only change this introduces is an extra $Z_{i,\downarrow} = 1 - 2\hat{n}_{i,\downarrow}$ operator in the hopping terms of $D(\theta)$ [see Eq. (7)].

The same behavior is observed for larger lattices: applying $D(\theta)$ to adjacent qubits encoding spin- \uparrow orbitals leads to no improvement of the fidelity relative to the exact ground state, but introducing the qubit storing the occupation of the spin- \downarrow orbital between them does allow for an enhancement of the overlap. Interestingly, while the Z strings arising from the

anticommutativity of fermionic operators are often regarded as inconvenient because they convert local fermionic operators into nonlocal qubit operations, here the $Z_{i,\downarrow} = 1 - 2\hat{n}_{i,\downarrow}$ introduced in the spin- \uparrow hopping terms [see Eq. (7)] was useful.

APPENDIX D: ADDING DOUBLON-HOLON PAIRS: OPTIMAL PARAMETER VALUE IS IDENTICAL REGARDLESS OF LATTICE SIZE

Figure 6 shows the optimal value of the free parameter θ against the interaction strength $\frac{U}{t}$ for the chains and ladders of different sizes considered in this work. Not only is the θ vs $\frac{U}{t}$ profile a simple convex curve for all geometries, but there is a nearly perfect matching of the quantitative values for lattices with the same geometry but different sizes. Hence, this parameter does not even require explicit optimization through a hybrid (quantum-classical) scheme: the optimal value for larger systems that cannot be simulated on conventional hardware can be simply obtained from the *in silico* simulations of smaller systems. In fact, the results presented in Fig. 4 for a 12-site chain (a) and ladder (b) were produced using the optimal parameter θ obtained from the analogous simulations on 10-site lattices.

[1] S. McArdle, S. Endo, A. Aspuru-Guzik, S. C. Benjamin, and X. Yuan, *Rev. Mod. Phys.* **92**, 015003 (2020).
[2] Y. Cao, J. Romero, J. P. Olson, M. Degroote, P. D. Johnson, M. Kieferová, I. D. Kivlichan, T. Menke, B. Peropadre, N. P. D. Sawaya, S. Sim, L. Veis, and A. Aspuru-Guzik, *Chem. Rev.* **119**, 10856 (2019).
[3] A. Auerbach, *Interacting Electrons and Quantum Magnetism* (Springer, New York, 1994).
[4] W. M. C. Foulkes, L. Mitas, R. J. Needs, and G. Rajagopal, *Rev. Mod. Phys.* **73**, 33 (2001).
[5] U. Schollwöck, *Rev. Mod. Phys.* **77**, 259 (2005).
[6] C. Cade, L. Mineh, A. Montanaro, and S. Stanisic, *Phys. Rev. B* **102**, 235122 (2020).

[7] Z. Cai, *Phys. Rev. Appl.* **14**, 014059 (2020).
[8] J. Preskill, *Quantum* **2**, 79 (2018).
[9] M. C. Gutzwiller, *Phys. Rev. Lett.* **10**, 159 (1963).
[10] J. Hubbard and B. H. Flowers, *Proc. R. Soc. A: Math. Phys. Eng. Sci.* **276**, 238 (1963).
[11] J. Kanamori, *Prog. Theor. Phys.* **30**, 275 (1963).
[12] D. P. Arovas, E. Berg, S. A. Kivelson, and S. Raghu, *Annu. Rev. Condens. Matter Phys.* **13**, 239 (2022).
[13] B. Murta and J. Fernández-Rossier, *Phys. Rev. B* **103**, L241113 (2021).
[14] D. Wecker, M. B. Hastings, N. Wiebe, B. K. Clark, C. Nayak, and M. Troyer, *Phys. Rev. A* **92**, 062318 (2015).

- [15] K. Seki, Y. Otsuka, and S. Yunoki, *Phys. Rev. B* **105**, 155119 (2022).
- [16] W. Heisenberg, *Z. Phys.* **49**, 619 (1928).
- [17] W. Kohn, *Rev. Mod. Phys.* **71**, 1253 (1999).
- [18] P. W. Anderson, *Phys. Rev. Lett.* **18**, 1049 (1967).
- [19] J. R. McClean, S. Boixo, V. N. Smelyanskiy, R. Babbush, and H. Neven, *Nat. Commun.* **9**, 4812 (2018).
- [20] M. Cerezo, A. Arrasmith, R. Babbush, S. C. Benjamin, S. Endo, K. Fujii, J. R. McClean, K. Mitarai, X. Yuan, L. Cincio, and P. J. Coles, *Nat. Rev. Phys.* **3**, 625 (2021).
- [21] A. Peruzzo, J. McClean, P. Shadbolt, M.-H. Yung, X.-Q. Zhou, P. J. Love, A. Aspuru-Guzik, and J. L. O’Brien, *Nat. Commun.* **5**, 4213 (2014).
- [22] K. Seki, T. Shirakawa, and S. Yunoki, *Phys. Rev. A* **101**, 052340 (2020).
- [23] P. Jordan and E. Wigner, *Z. Phys.* **47**, 631 (1928).
- [24] E. Lieb and D. Mattis, *J. Math. Phys.* **3**, 749 (1962).
- [25] J. Kattemölle and J. van Wezel, *Phys. Rev. B* **106**, 214429 (2022).
- [26] J. L. Bosse and A. Montanaro, *Phys. Rev. B* **105**, 094409 (2022).
- [27] H. Yu, Y. Zhao, and T.-C. Wei, *Phys. Rev. Res.* **5**, 013183 (2023).
- [28] E. Farhi, J. Goldstone, and S. Gutmann, [arXiv:1411.4028](https://arxiv.org/abs/1411.4028).
- [29] D. Wecker, M. B. Hastings, and M. Troyer, *Phys. Rev. A* **92**, 042303 (2015).
- [30] P. Anderson, *Mater. Res. Bull.* **8**, 153 (1973).
- [31] P. W. Anderson, *Science* **235**, 1196 (1987).
- [32] See Supplemental Material at <http://link.aps.org/supplemental/10.1103/PhysRevB.109.035128> for a pedagogical introduction to the structure of the RVB-inspired ansatz adopted in the first step, analogous results to those presented in Fig. 2 for one-dimensional lattices with periodic boundary conditions, and analogous results to those presented in Fig. 4 for smaller lattices with the same geometry, including the confirmation of the increase of the double occupancy of lattice sites as the interaction strength U/t decreases.
- [33] P. Weinberg and M. Bukov, *QuSpin: A Python package for dynamics and exact diagonalization of quantum many-body systems* (2017), last accessed on 16-10-2023.
- [34] I. D. Kivlichan, J. McClean, N. Wiebe, C. Gidney, A. Aspuru-Guzik, G. K.-L. Chan, and R. Babbush, *Phys. Rev. Lett.* **120**, 110501 (2018).
- [35] Z. Jiang, K. J. Sung, K. Kechedzhi, V. N. Smelyanskiy, and S. Boixo, *Phys. Rev. Appl.* **9**, 044036 (2018).
- [36] It does not matter what this operation does to the basis states $|10\rangle$ and $|11\rangle$, because they will have zero amplitude in the input state, as the ancilla is provided in $|0\rangle$.
- [37] The phrase “most significant qubit” refers to the binary decomposition of the labels of the rows and columns of the matrices of the unitary operation. If the rows/columns are labeled (from top to bottom / left to right) as $\{0, 1, 2, 3\}$, or $\{00, 01, 10, 11\}$ in binary form, then the leftmost bit is the most significant, so the first two rows/columns are associated with the corresponding qubit in state “0” and the last two rows/columns are associated with this qubit in state “1”.
- [38] F. Verstraete, J. I. Cirac, and J. I. Latorre, *Phys. Rev. A* **79**, 032316 (2009).
- [39] D. Baeriswyl, *Found. Phys.* **30**, 2033 (2000).
- [40] H. Bethe, *Z. Phys.* **71**, 205 (1931).
- [41] J. S. Van Dyke, G. S. Barron, N. J. Mayhall, E. Barnes, and S. E. Economou, *PRX Quantum* **2**, 040329 (2021).
- [42] A. Sopena, M. H. Gordon, D. García-Martín, G. Sierra, and E. López, *Quantum* **6**, 796 (2022).
- [43] C. K. Majumdar and D. K. Ghosh, *J. Math. Phys.* **10**, 1388 (1969).
- [44] C. K. Majumdar and D. K. Ghosh, *J. Math. Phys.* **10**, 1399 (1969).
- [45] B. Sriram Shastry and B. Sutherland, *Physica B+C* **108**, 1069 (1981).
- [46] P. Corboz and F. Mila, *Phys. Rev. B* **87**, 115144 (2013).
- [47] A. W. Cross, L. S. Bishop, J. A. Smolin, and J. M. Gambetta, [arXiv:1707.03429](https://arxiv.org/abs/1707.03429).
- [48] The Scipy Community, *SciPy Optimize: Minimize Documentation* (2008), last accessed on 16-10-2023.